# Airborne observations of clouds in the Central Arctic during the Multidisciplinary drifting Observatory for the Study of Arctic Climate (MOSAiC) expedition

**Klingebiel, M.[1], Ehrlich, A.[1], Schäfer, M.[1], Becker, S.[1], Jäkel, E.[1] Wendisch, M.[1]**

[1] *Institute of Meteorology, Stephanstr. 3, 04103 Leipzig,*
*E-mail: marcus.klingebiel@uni-leipzig.de*

**Summary:** In August and September 2020, a group from the Leipzig Institute for Meteorology (LIM) participated in the research campaign MOSAiC-ACA. During this campaign the Polar 5 research aircraft was used to identify the cloud characteristics and their impact on the radiative energy budget, which are relevant for the role of clouds in Arctic amplification in the vicinity of Svalbard. In this report we will give an overview about the campaign and the instruments operated by LIM and point out the challenges which we faced while performing a research campaign in the middle of a global pandemic and in an Arctic environment with the second lowest sea ice coverage in the last 42 years.

**Zusammenfassung:** Im August und September 2020 hat eine Gruppe vom Leipziger Institut für Meteorologie (LIM) an der Forschungskampagne MOSAiC-ACA teilgenommen, um unter Verwendung des Forschungsflugzeuges Polar 5 die relevanten Wolkencharakteristiken und deren Einfluss auf das Strahlungsbudget zu identifizieren. Diese spielen eine Rolle bei der Arktischen Verstärkung in der Umgebung von Spitzbergen. In diesem Bericht geben wir eine Übersicht über die Kampagne und die Instrumente, die vom LIM verwendet wurden und erläutern die Herausforderungen, die uns während der Forschungskampagne in Mitten einer globalen Pandemie und in einer Arktischen Umgebung, in der die Eisbedeckung die zweitniedrigste innerhalb der letzten 42 Jahre war, begegneten.

## 1 Introduction

Throughout the last years, the Arctic experienced an enhanced warming, which is known as Arctic amplification. This process leads to e.g. a decrease in the amount of Arctic sea ice. To identify the role of clouds in Arctic amplification, we carried out the MOSAiC-Airborne observations in the Central Arctic (MOSAiC-ACA) campaign in August and September 2020 in the vicinity of Svalbard (Spitsbergen), which is related to the Multidisciplinary drifting Observatory for the Study of Arctic Climate (MOSAiC) expedition and the Transregional Collaborative Research Center ArctiC Amplification: Climate relevant Atmospheric and SurfaCe Processes, and Feedback Mechanisms ((AC)$^3$,Wendisch et al. (2021)). Figure 1 shows the tracks of all nine flights performed during the MOSAiC-ACA campaign including the Arctic sea ice coverage of September 2020 and the positions of the launched dropsondes.

The MOSAiC-ACA campaign extends the Arctic cloud measurements from the previous Arctic CLoud Observations Using airborne measurements during polar Day (ACLOUD, Wendisch et al. (2019)) and Airborne measurements of radiative and turbulent FLUXes (AFLUX) campaigns, which were conducted in May/June 2017 and March/April 2019, respectively.

When we planned the campaign, we did not expect such a low sea ice concentration for this time of year, which was quantified by the National Snow and Ice Data Center (NSIDC, 2020) to be the second lowest in the 42-year satellite record, behind only September 2012. This made the campaign very challenging, because the focus of our research is the marginal sea ice zone and therefore we need to be able to reach the ice with the research aircraft. On the other hand, this low sea ice concentration shows how urgent it is to collect atmospheric observations in this area to better understand the role of clouds and their radiative properties in a future ice-free environment.

What we also didn't expect in 2020 was the COVID-19 pandemic, which made it very challenging to perform a research campaign in a foreign country. Nevertheless, thanks to all our partners involved in the $(AC)^3$ project (see `http://www.ac3-tr.de` for more information), especially the administration of AWI, it was possible to realize the campaign, despite a lot of restrictions and requirements. To successfully carry out this campaign, only a small but highly motivated crew of 27 researchers, engineers and pilots managed flight operation, weather forecast, instrument operation and data handling. Even there was a second research aircraft involved in the campaign to measure sea ice concentrations, namely the Polar 6, we will only focus in this report on the atmospheric measurements from the Polar 5 aircraft, which was equipped with in-situ and remote sensing instruments to characterize Arctic boundary layer clouds. These measurements will primarily address seasonal differences by considering the previous campaigns in the scope of $(AC)^3$ and build the bridge between the ground-based observations of the Research Vessel (RV) Polarstern, the research station at Ny-Ålesund and satellite observations.

## 2 Aircraft and instruments

The Polar 5 aircraft is a Basler BT-67, which is specially modified to fly under extreme polar conditions. With advanced navigation systems, de-icing systems and landing gear, which combine skis and conventional tires, the aircraft can operate in severe weather conditions with temperatures down to -54°C (Wesche et al., 2016). During the MOSAiC-ACA campaign, the Polar 5 was equipped with several in-situ and remote sensing instruments to measure atmospheric parameters, the radiative energy budget and as well as cloud micro- and macrophysical properties. In addition, the Polar 5 is equipped with a dropsonde system, which allows for the launch of Vaisala RD-41 sondes to measure vertical profiles of temperature, humidity, pressure and winds. In this report, we will focus on the remote sensing instruments from LIM, which will be introduced in the following section.

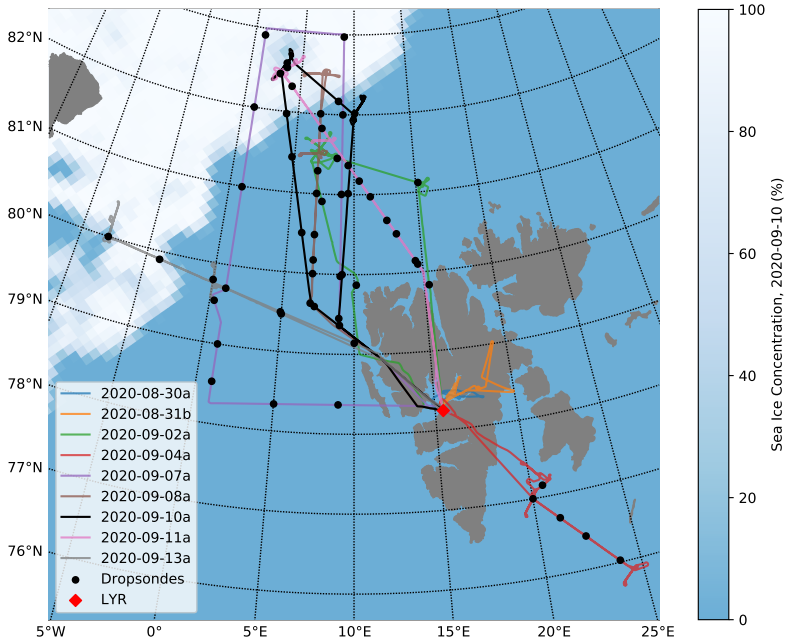


Figure 1: *Polar 5 flight tracks during the MOSAiC-ACA campaign. All in all, nine flights were conducted in the vicinity of Svalbard and 60 dropsondes were launched. All flights were performed from Longyearbyen Airport (LYR) located on the Svalbard archipelago. The sea ice concentration is based on AMSR-Satellite data and is the second lowest in the 42 years of satellite record.*

### 2.1 SMART Albedometer

During MOSAiC-ACA the Spectral Modular Airborne Radiation measurement sysTem (SMART) was configured to measure the spectral solar irradiance and radiance. For this purpose, four optical inlets are mounted at the aircraft fuselage and connected via optical fibers to grating spectrometers dispersing the incident radiation, which is detected by a single-line photodiode array. SMART covers a spectral range between 300 nm and 2200 nm wavelength and contains two optical shutters, which allow necessary simultaneous dark measurements for the spectrometers (Wendisch et al., 2019; Ehrlich et al., 2019).

### 2.2 AISA Hawk spectral imager

The Airborne Imaging Spectrometer for Applications (AISA) Hawk instrument (Pu, 2017; Ehrlich et al., 2019) consists of a downward-viewing push broom sensor aligned across the flight track to measure 2D fields of upward radiance. The push broom sensor contains 384 across-track pixels, where each pixel performs spectral measurements between the wavelength range of 930 nm and 2550 nm in 288 channels. With a 36° field of view (FOV) and a sampling frequency of 20 Hz, the instrument has a spatial resolution of 2 m, assuming a distance between aircraft and cloud of 1 km (Ruiz-Donoso et al., 2020).

### 2.3 AISA Eagle spectral imager

The AISA Eagle instrument is the second imaging spectrometer installed on Polar 5. It uses a measurement approach similar to AISA Hawk but focuses on shorter wavelengths with higher spectral and spatial resolution. With a single line push broom sensor consisting of 1024 across-track pixels measurements of 2D fields of upward radiance are performed in 488 channels covering a wavelength range between 400 nm and 970 nm. The FOV is 36.3° and delivers a spatial resolution below 1 m for a target at a distance of 1 km (Schäfer et al., 2015). During MOSAiC-ACA it was operated with a frame rate of 20 Hz to acquire an along-track spatial resolution comparable to that of AISA Hawk.

### 2.4 Nikon

A commercial digital camera (Nikon D5) measured the directional distribution of upward radiance in three spectral channels (RGB) of the lower hemisphere every 6 s. The camera was either equipped with a wide-angle lens (up to flight 8) or a fisheye-lens (flight 9 to flight 11). The two configurations allowed the cloud and surface observations of a large area within a FOV of 80° x 100° (wide-angle lens) and about 150° when using the fisheye-lens. The camera was fully calibrated with respect to its radiometric, geometric and spectral characteristics. The images were recorded in raw data format to gain the full dynamic range (14 bit) of the camera sensor chip with a spatial resolution of 5584 x 3728 pixels.

Nadir radiances measured by SMART, AISA Eagle, and Nikon from flight 9 (10 September 2020) were compared to verify the individual calibrations. During a period of three hours, observations of cloud tops, cloud profiles, and sea ice were performed which cover a broad range of different reflectivity. Combining the three instruments needs to account for the different spatial, temporal, and spectral resolutions. SMART and AISA Eagle spectra were convoluted with respect to the spectral response functions of the three spectral channels of the Nikon camera. AISA Eagle and Nikon data were spatially averaged to match the size of the SMART footprint of 2°. Figure 2 displays scatterplots of the radiance data using SMART as a reference. The correlation between SMART and AISA Eagle data (red dots) is consistent for all three channels with a correlation coefficient (R) of about 0.97 and an offset of 6%, which falls within the measurement uncertainty of the two instruments. The correlation coefficient between SMART and Nikon data is slightly lower with R = 0.94. The best agreement was found for the red and the green channels, while a significant offset of about 22% was derived for the blue channel. Finally, these findings were used to inter-calibrate the Nikon camera in order to provide a consistent data set.

### 2.5 Broadband solar and terrestrial radiation

Up- and downward broadband irradiances are obtained by using pairs of CMP 22 pyranometers and CGR4 pyrgeometers. The pyranometers cover a solar wavelength range between 0.2 and 3.6 µm, while the pyrgeometers cover a thermal infrared wavelength range between 4.5 and 42 µm. The sampling frequency is 20 Hz and the uncertainty of the sensors is less than 3% (Gröbner et al., 2014). To adjust the misalignment of the aircraft during flight for the downward direct solar irradiance, a method from Bannehr

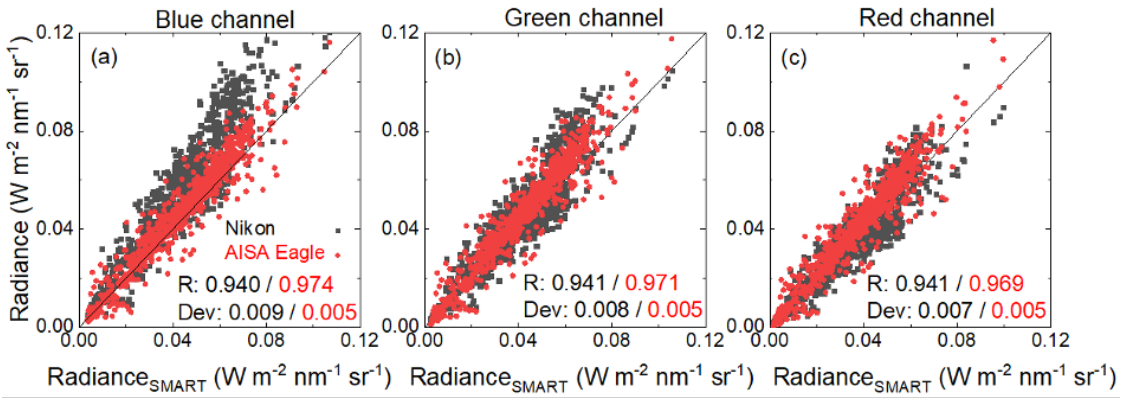


Figure 2: *Comparison of radiances in nadir direction measured by SMART, Nikon, and AISA Eagle on 10 September 2020. "Dev" represents the root mean squared error between the reference radiance of SMART and the radiances by Nikon (black) and AISA Eagle (red), respectively. R indicates the Pearson's correlation coefficient.*

Table 1: *Research flights in the vicinity of Svalbard with the number of dropsondes, the number of pictures recorded by the Nikon camera, the measurement time of each instrument and the total amount of the recorded data for each flight in Gigabytes (GB).*

| | | | | | Measurement time | | | | |
|---|---|---|---|---|---|---|---|---|---|
| **Flight #** | **Date** | **Flight duration** | **Dropsondes** | **Nikon pictures** | **Eagle** | **Hawk** | **Broadband** | **SMART** | **Data (GB)** |
| 2 | 30.08.2020 | 0h 53m | - | 342 | 0h 15m | 0h 39m | 0h 53m | 0h 21m | 22.7 |
| 4 | 31.08.2020 | 2h 15m | - | 4273 | 0h 49m | 1h 51m | 2h 15m | 2h 13m | 216.5 |
| 5 | 02.09.2020 | 5h 31m | 6 | 3120 | 2h 31m | 2h 25m | 5h 31m | 5h 29m | 277.3 |
| 6 | 04.09.2020 | 5h 31m | 5 | 3107 | 1h 46m | 1h 42m | 5h 31m | 0h 22m | 214.2 |
| 7 | 07.09.2020 | 5h 41m | 14 | 3476 | 4h 13m | 3h 33m | 5h 41m | 5h 41m | 410.4 |
| 8 | 08.09.2020 | 6h 05m | 7 | 5517 | 2h 25m | 2h 21m | 6h 05m | 6h 05m | 318,5 |
| 9 | 10.09.2020 | 6h 16m | 11 | 4738 | 4h 27m | 4h 21m | 6h 16m | 6h 16m | 475,6 |
| 10 | 11.09.2020 | 5h 40m | 10 | 6063 | 1h 56m | 1h 52m | 5h 40m | 4h 20m | 292,1 |
| 11 | 13.09.2020 | 5h 46m | 7 | 5640 | 1h 39m | 1h 36m | 5h 46m | 5h 46m | 261.4 |
| | **Total:** | **44h 17m** | **60** | **36276** | **20h 01m** | **20h 20m** | **44h 17m** | **36h 33m** | **2489** |

and Schwiesow (1993) and Boers et al. (1998) is applied. More specific details about these broadband solar and terrestrial radiation instruments operated on Polar 5 are given by Ehrlich et al. (2019).

## 3 Remote sensing measurements

During the campaign we performed 11 flights. The first flight was a test flight in Bremerhaven, Germany and the third flight was used for certification purposes, where the instruments were not switched on. The other flights in the vicinity of Svalbard are listed in Table 1, together with the flight duration, the number of launched dropsondes, the number of pictures recorded by the Nikon camera, the measurement time of each instrument and the amount of data recorded for each flight. In total, 2.5 TB were recorded by the remote sensing instruments from LIM.

In the following, we will focus on the remote sensing measurements from research flight 9 (the associated flight track is marked in black in Figure 1), which had the main purpose to investigate the differences of cloud properties over sea ice and open water. For this reason, the Polar 5 headed first to the north over the sea ice (82.5°N, 0.3°E) and

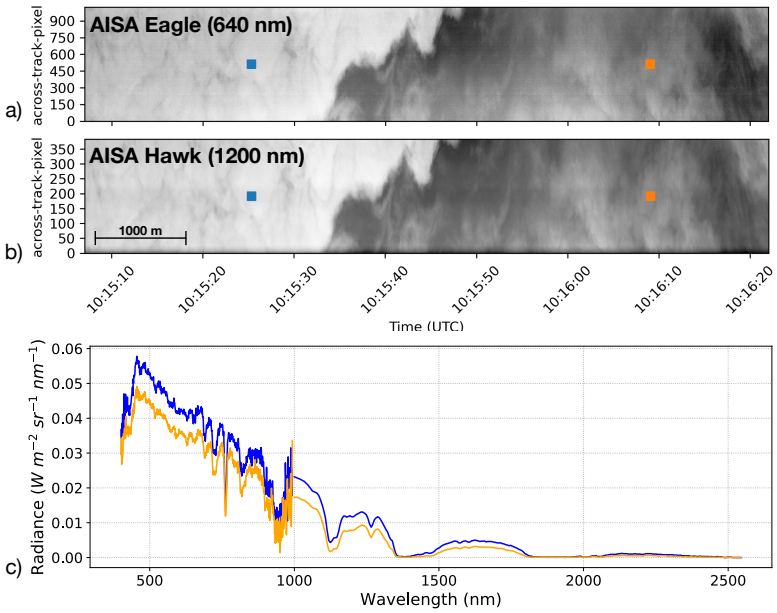


Figure 3: *2D fields of upward radiances, sampled by the AISA Eagle (a) and AISA Hawk (b) instrument. Spectral radiances at the locations marked with the square in (a) and (b) are given in panel (c) and show a combination of both instruments.*

sampled two cloud layers there, one ice cloud between 8600 and 8900 ft (2.6 and 2.7 km) and one liquid water cloud reaching from the ground to 5000 ft (1.5 km). Afterwards, the Polar 5 headed towards the open ocean (82°N, 10°E) and sampled a cloud reaching from the surface up to ~3000 ft (~900 m). Both cloud systems were probed in a staircase pattern.

A measurement example of AISA Eagle and AISA Hawk is given in Figure 3, which shows approximately one minute (~10 km) of measurements during flight 9 on 10 September 2020. During this flight section, the edge of a boundary layer cloud over open water was sampled with both instruments. This cloud edge is visible in Figure 3a and 3b between 10:15:30 UTC and 10:15:50 UTC. To demonstrate the capabilities of the spectral imagers, Figure 3c shows two combined AISA Eagle and AISA Hawk spectra for the center pixels marked by the blue and orange rectangles in Figure 3a and 3b. The spectra show higher radiance over the boundary layer cloud (blue rectangle) and lower radiance over a thinner cloud (orange rectangle). The spectra sampled by the AISA Hawk instrument (between 930 nm and 2550 nm) look smoother than from AISA Eagle due to the different spectral resolutions of both imagers.

Another example, given in Figure 4, shows the differences in broadband radiative cloud properties over Arctic sea ice (left panels) and open ocean (right panels). The albedo values exceeding 1 in Fig. 4c are due to horizontal photon transport. While the net terrestrial irradiance (orange line) is very similar over ice (Figure 4a) and over ocean (Figure 4b), the differences in the net solar irradiance are remarkable. Over ocean the net solar irradiance is 33 W $m^{-2}$ higher than over Arctic ice. The cloud albedo, which is the ratio of the solar upward and downward irradiance, is higher over Arctic ice (Figure 4c) than over ocean (Figure 4d). This is plausible, because the ice surface reflects more solar radiation than the ocean. We will use these kind of measurements to analyze the typical

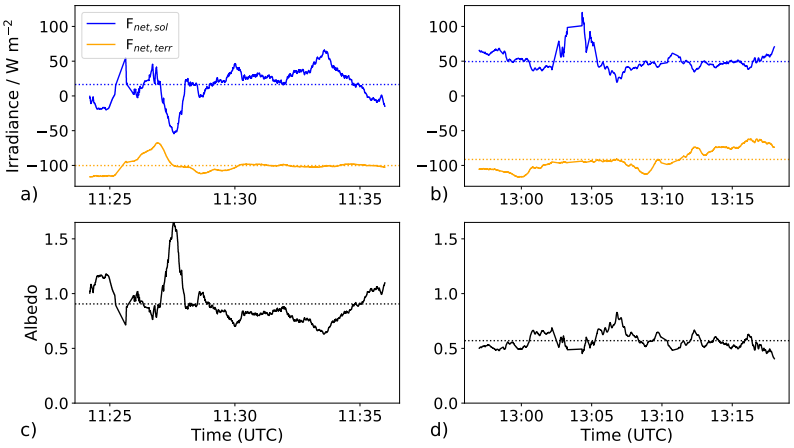


Figure 4: *Net solar and terrestrial irradiance over sea ice (a) and open ocean (b). The corresponding albedo over sea ice and open ocean is given in (c) and (d), respectively. The dotted lines indicate the mean value of each parameter.*

conditions over Arctic sea ice and open ocean in further studies. Combining the data from the MOSAiC-ACA campaign with those of the ACLOUD and AFLUX campaign will provide us with the opportunity to identify seasonal differences of the cloud radiative properties.

## 4 Conclusion and next steps

In August and September 2020, nine research flights with a total flight time of 44 hours were performed with the Polar 5 aircraft to study the cloud characteristics and their impact on the radiative energy budget, that are relevant for the role of clouds in Arctic amplification. First results from the spectral imagers and the broadband solar and terrestrial radiation measurements look very promising. The data indicate the spectral differences between different types of clouds and the differences over Arctic ice and ocean. Although we present only a very small part of the data, they show that the instruments were working properly, and we can use the data to reach more advanced scientific goals. In particular, we will use this dataset to analyze the different cloud properties over Arctic sea ice and ocean and will compare them with previous $(AC)^3$ campaigns as well as satellite observations and data from the RV Polarstern.

## Acknowledgements

We gratefully acknowledge the funding by the Deutsche Forschungsgemeinschaft (DFG, German Research Foundation) – Project Number 268020496 5 – TRR 172, within the Transregional Collaborative Research Center “ArctiC Amplification: Climate Relevant Atmospheric and SurfaCe Processes, and Feedback Mechanisms $(AC)^3$.

## References

Bannehr, L. and Schwiesow, R.: A Technique to Account for the Misalignment of Pyranometers Installed on Aircraft, Journal of Atmospheric and Oceanic Technology, 10, 774 – 777, doi:10.1175/1520-

0426(1993)010<0774:ATTAFT>2.0.CO;2, 1993.

Boers, R., Mitchell, R. M., and Krummel, P. B.: Correction of aircraft pyranometer measurements for diffuse radiance and alignment errors, Journal of Geophysical Research: Atmospheres, 103, 16 753–16 758, doi:10.1029/98JD01431, 1998.

Ehrlich, A., Wendisch, M., Lüpkes, C., et al.: A comprehensive in situ and remote sensing data set from the Arctic CLoud Observations Using airborne measurements during polar Day (ACLOUD) campaign, Earth System Science Data, 11, 1853–1881, doi:10.5194/essd-11-1853-2019, 2019.

Gröbner, J., Reda, I., Wacker, S., et al.: A new absolute reference for atmospheric longwave irradiance measurements with traceability to SI units, Journal of Geophysical Research: Atmospheres, 119, 7083–7090, doi:10.1002/2014JD021630, 2014.

NSIDC: Arctic sea ice decline stalls out at second lowest minimum, URL http://nsidc.org/arcticseaicenews/2020/09/, 2020.

Pu, R.: Hyperspectral Remote Sensing: Fundamentals and Practices (1st ed.), CRC Press., doi:10.1201/9781315120607, 2017.

Ruiz-Donoso, E., Ehrlich, A., Schäfer, M., et al.: Small-scale structure of thermodynamic phase in Arctic mixed-phase clouds observed by airborne remote sensing during a cold air outbreak and a warm air advection event, Atmospheric Chemistry and Physics, 20, 5487–5511, doi:10.5194/acp-20-5487-2020, 2020.

Schäfer, M., Bierwirth, E., Ehrlich, A., Jäkel, E., and Wendisch, M.: Airborne observations and simulations of three-dimensional radiative interactions between Arctic boundary layer clouds and ice floes, Atmospheric Chemistry and Physics, 15, 8147–8163, doi:10.5194/acp-15-8147-2015, 2015.

Wendisch, M., Macke, A., Ehrlich, A., et al.: The Arctic Cloud Puzzle: Using ACLOUD/PASCAL Multiplatform Observations to Unravel the Role of Clouds and Aerosol Particles in Arctic Amplification, Bulletin of the American Meteorological Society, 100, 841 – 871, doi:10.1175/BAMS-D-18-0072.1, 2019.

Wendisch, M., Handorf, D., Tegen, I., Neggers, R. A. J., and Spreen, G.: Glimpsing the ins and outs of the Arctic atmospheric cauldron, Eos, 102, doi:10.1029/2021EO155959, 2021.

Wesche, C., Steinhage, D., and Nixdorf, U.: Polar aircraft Polar5 and Polar6 operated by the Alfred Wegener Institute, Journal of large-scale research facilities Facilities, 2, doi:10.17815/jlsrf-2-153, 2016.